



REGENERATION

Charting a high-resolution roadmap for regeneration of pancreatic β cells by in vivo transdifferentiation from adult acinar cells

Gang Liu^{1,2†}, Yana Li^{3,4†}, Mushan Li^{5†}, Sheng Li^{1,2}, Qing He^{1,2}, Shuxin Liu^{1,2}, Qiang Su^{1,2}, Xiangyi Chen^{1,2}, Minglu Xu^{1,2}, Zhen-Ning Zhang^{1,2*}, Zhen Shao^{3*}, Weida Li^{1,2,6*}

Adult mammals have limited capacity to regenerate functional cells. Promisingly, in vivo transdifferentiation heralds the possibility of regeneration by lineage reprogramming from other fully differentiated cells. However, the process of regeneration by in vivo transdifferentiation in mammals is poorly understood. Using pancreatic β cell regeneration as a paradigm, we performed a single-cell transcriptomic study of in vivo transdifferentiation from adult mouse acinar cells to induced β cells. Using unsupervised clustering analysis and lineage trajectory construction, we uncovered that the cell fate remodeling trajectory was linear at the initial stage and the reprogrammed cells either evolved to induced β cells or toward a “dead-end” state after day 4. Moreover, functional analyses identified both *p53* and *Dnmt3a* that acted as reprogramming barriers during the process of in vivo transdifferentiation. Collectively, we decipher a high-resolution roadmap of regeneration by in vivo transdifferentiation and provide a detailed molecular blueprint to facilitate mammalian regeneration.

INTRODUCTION

The limited regenerative capacity of injured adult mammalian cells leads to irreversible organ damage. To realize the regeneration of functional cells for preventing and treating disease, numerous studies are therefore focusing on developing regenerative medicine. Notably, studies have shown that cellular reprogramming is a promising approach for regenerative medicine, including pluripotent reprogramming and transdifferentiation (1, 2). Through ectopic expression of lineage-specific transcription factors (TFs), terminally differentiated fibroblasts could be reprogrammed into induced pluripotent stem cells (iPSCs) or directly reprogrammed into functional cardiomyocytes or neurons in vitro (3–5). In addition, the adult mouse pancreatic exocrine cells were first reprogrammed into β cells in vivo by adenoviral delivery of three TFs Mafa, Pdx1, and Ngn3 (hereafter called M3 factors) (6). Then, the cardiomyocyte-like cells and neurons were also regenerated by in vivo transdifferentiation based on the previous in vitro experimental strategy. The murine cardiac fibroblasts could be converted into cardiomyocyte-like cells through forced expression of *Gata4*, *Mef2c*, and *Tbx5* (7). The in vivo reprogramming of astrocytes into neurons and neuroblasts could be achieved via expressing *Ascl1*, *Brn2*, and *Myt1l* together and ectopic expression of *Sox2* alone, respectively (8, 9).

Meanwhile, to have a deep understanding of the cellular reprogramming process, single-cell RNA sequencing (scRNA-seq) has

been widely used for deciphering heterogeneity and molecular dynamics in multiple direct reprogramming cases. For instance, by using scRNA-seq, previous study revealed two distinct trajectories during the conversion process of fibroblasts to endoderm progenitors and found that the addition of methyltransferase *Mettl7a1* could improve the efficiency (10). During the conversion of fibroblasts to cardiomyocytes, single-cell transcriptomic analyses also revealed the cellular heterogeneity and identified *Ptbp1* as a previously unidentified reprogramming barrier (11). The single-cell transcriptomic study of conversion from fibroblasts to neurons dissected the reprogrammed cells that went through divergent intermediate states (12). These scRNA-seq studies of in vitro cellular reprogramming provided a highly precise dynamic of the transcriptome.

Furthermore, the transplantation of in vitro-reprogrammed cells is a promising approach for the development of cell replacement therapy. On the contrary, in vivo transdifferentiation heralds the possibility of regenerating disease-relevant cells without a transplantation procedure, taking place within the tissue-specific physiological niche, which is different from the in vitro culture conditions (13). However, the high-resolution molecular roadmap of in vivo transdifferentiation in mammals is poorly understood, limiting the application of this strategy for regenerative medicine.

Particularly, regenerating β cells in vivo from adult pancreatic acinar cells in the pancreas by coexpressing M3 factors provides a paradigm for regeneration (14). Meanwhile, the loss of β cell mass causes diabetes mellitus, suggesting that β cell regeneration may be a promising strategy for diabetes therapy (15). Although hyperglycemia in diabetic patients could be mitigated by insulin injection or chemical drugs, these treatments cannot regenerate β cells and efficiently cure diabetes (16, 17). In addition, human islet transplantation has been demonstrated as an effective treatment for diabetes but is hampered by the scarcity of donors (18). Hopefully, acinar

¹Translational Medical Center for Stem Cell Therapy and Institute for Regenerative Medicine, Shanghai East Hospital, Frontier Science Center for Stem Cell Research, School of Life Sciences and Technology, Tongji University, Shanghai 200092, China.

²Tsingtao Advanced Research Institute, Tongji University, Qingdao 266073, China.

³CAS Key Laboratory of Computational Biology, Shanghai Institute of Nutrition and Health, Chinese Academy of Sciences, Shanghai 200031, China.

⁴University of Chinese Academy of Sciences, Beijing 100049, China.

⁵Department of Statistics, The Pennsylvania State University, University Park, PA 16802, USA.

⁶Reg-Verse Therapeutics (Shanghai) Co. Ltd., Shanghai 200120, China.

*Corresponding author. Email: znzhang@tongji.edu.cn (Z.-N.Z.); shaozhen@picb.ac.cn (Z.S.); liweida@tongji.edu.cn (W.L.)

†These authors contributed equally to this work.

cells could offer an ideal source for the regeneration of β cells by in vivo transdifferentiation, because the acinar cells take up the most abundant population of cell type in the pancreas (19). Moreover, the pancreatic microenvironment promotes the maturation of regenerated β cells and the formation of islet-like structures in vivo (14). However, a high-resolution regenerative roadmap of in vivo transdifferentiation remains poorly understood. Especially the inherent barrier factors that block the cell fate conversion from acinar cells to β cells are less known.

Here, we performed scRNA-seq at multiple predetermined time points of the in vivo transdifferentiation from acinar cells to β cells that were triggered by M3 factors. By reconstructing the trajectory of cell fate evolution, we found that the trajectory of cell fate was homogeneous at the initial stage before day 4. Afterward, the heterogeneity of reprogrammed cells was presented along two distinct trajectories. One trajectory exhibited as a group of successfully converted β cells and the other one toward a dead-end state with relatively low expression of *Ins2* but high expression of acinar cell marker *Ptf1a*, indicating the failure of β cell regeneration. Furthermore, whole transcriptome analysis of reprogramming cells in the initial stage found some genes involved in cell cycle arrest were significantly up-regulated compared to cells of transdifferentiation origin. Functional assays confirmed that cell cycle arrest regulator *p53* severed as a barrier at the initial stage. We further demonstrated that *Dnmt3a* also acted as a barrier during the process of transdifferentiation. High expression of *Dnmt3a* effectively inhibited M3 factor-induced β cell regeneration, and knockdown of *Dnmt3a* significantly increases the efficiency. These findings decipher a high-resolution roadmap of in vivo transdifferentiation from adult acinar cells to β cells and offer previously unidentified regulate targets for β cell regeneration in vivo.

RESULTS

scRNA-seq temporally reveals dynamic transcriptional remodeling during acinar cell to β cell transdifferentiation in vivo

The previous study demonstrated that adult mouse acinar cells could be converted into functional β cells in vivo through ectopic expressing M3 factors (14). In addition, the intensity of insulin staining in induced β cells was consistent with endogenous islet β cells on day 10 (6). To decipher a high-resolution molecular roadmap of β cell regeneration by in vivo transdifferentiation, we performed scRNA-seq at multiple predetermined time points from day 0 to 10 during the process of transdifferentiation. The M3 factor-expressing cells were labeled with fluorescent protein mCherry through adenoviral delivery. On the basis of this, the reprogrammed single cells were sorted for scRNA-seq library construction via fluorescence-activated cell sorting (FACS). The single acinar cells from no-treatment mice were collected for library construction as control and defined as the original point (day 0) of transdifferentiation (Fig. 1A). In total, we harvested 3648 single cells from seven time points for library construction, and 2641 high-quality single-cell profiles were retained for downstream analysis (fig. S1, A and B).

Dimensional reduction analysis using uniform manifold approximation and projection (UMAP) revealed a diversity of cell types. Unsupervised clustering analysis identified 10 distinct cell clusters (clusters A to J) (Fig. 1B). Combining with the time point

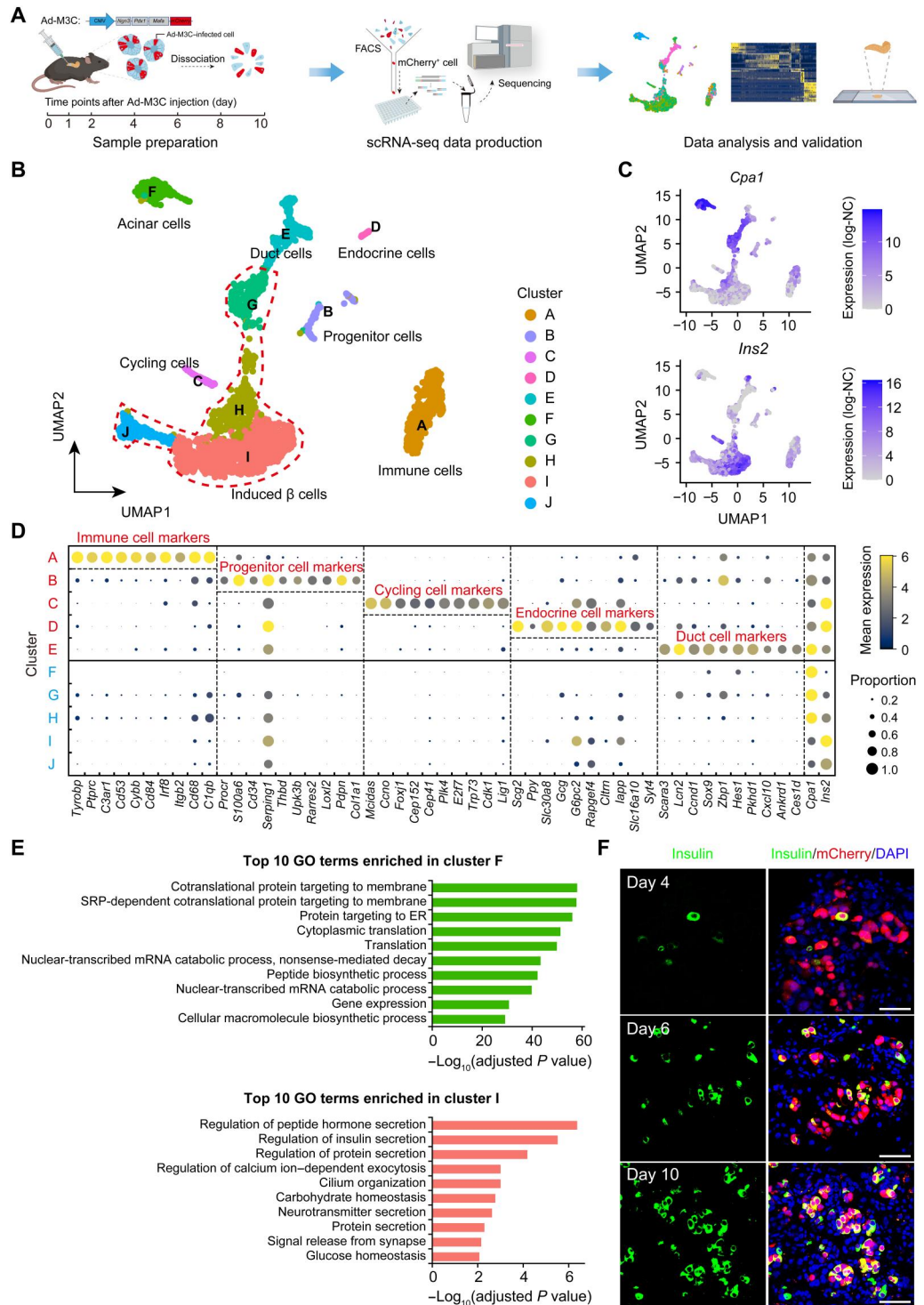
information of cells, clusters from F to J presented the transdifferentiation route of cells from day 0 to 10 (fig. S1C). Notably, the expression of acinar cell marker gene *Cpa1* gradually decreased over the time points, while the expression of β cell marker gene *Ins2* gradually increased over the time points (Fig. 1C). In cluster F, 99.6% of cells were from day 0 and had the highest expression of *Cpa1*, so they were annotated as acinar cells (Fig. 1, C and D; and fig. S1D), and gene ontology (GO) terms about acinar cells enriched by up-regulated genes also approved that (Fig. 1E). Cluster I was likely to include induced β cells due to relatively high expression of *Ins2* (Fig. 1, C and D; and fig. S1E), and enriched GO terms by up-regulated genes were associated to β cell functions (Fig. 1E). In addition, the results of immunofluorescence staining also showed that Insulin⁺mCherry⁺ cells (induced β cells) were gradually increased along the timeline (Fig. 1F). These results suggested that the cells in cluster F, which were acinar cells, and the cells in the continuous clusters from G to J were the cells that actually exhibit the process of transdifferentiation from acinar cells to β cells.

Furthermore, we figured out the identity of cells in other separated clusters from A to E. According to the expression of up-regulated genes and enriched biological functions of these clusters, we annotated cluster A (with high expression of *Cd68*) as immune cells; cluster B (with high expression of *Cd34*) as progenitor cells; cluster C (with high expression of *Cdk1*) as cycling cells; cluster D (with high expression of *Gcg*, *Ins2*, *Sst*, and *Ppy*), which is a minor cluster, as contamination of intrinsic endocrine cells; and cluster E (with high expression of *Sox9*) as duct cells (Fig. 1D and fig. S1, E and F). Above all, we focused on the cells from clusters F to J for analyzing the entire process of gradual conversion from acinar cells to β cells. Last, we picked 1855 cells that were included in cluster F (acinar cells as control) and continuously changed clusters from clusters G to J for downstream analysis.

Trajectory reconstruction reveals the heterogeneity of cell fate during the process of transdifferentiation

The trajectory of cell fate conversion from adult acinar cells to β cells remains a mystery. To decipher the trajectory of reprogramming cells during the transdifferentiation from acinar cells to β cells, we first visualized the overall situation of the retained 1855 cells and reclustered them into more elaborate 10 clusters (C0 to C9), where cells in C1 to C8 were distributed continuously along the timeline (Fig. 2A and fig. S2A). Among these 10 clusters, cells in C9 were considered as outliers and were excluded from further analysis. Obviously, C0 (acinar cells, the origin of transdifferentiation) is quite separated from the other cells along the axis of UMAP1, suggesting the rapid and marked changes in transcriptome profiles after expressing M3 factors. Then, cells in C1 to C8, those continuously changing cells, were selected for trajectory construction using Slingshot (20). We found two different lineages and estimated cell level pseudotime along these two lineages (Fig. 2, B and C). The lineage 1 started from C1 to C5 and then turned to C6. While the lineage 2 started from C1 to C5 and then turned to C7 and C8 (Fig. 2C and fig. S2B). Lineage 1-specific cluster (C6) and lineage 2-specific clusters (C7 and C8) contained cells from the last four time points of sample collection from day 4 to 10, and there was no obvious chronological difference between the endpoints of the two lineages, C6 and C8 (Fig. 2D and fig. S2B). These results suggested that C5 was the branching point of the trajectory, leading to C6 and C8, respectively, likely corresponding to two different cell

Fig. 1. scRNA-seq of captured cells during the in vivo transdifferentiation process from pancreatic acinar cells to β cells. (A) Schematic diagram of experimental design. Adenovirus-infected (Ad-M3C, M3 factors expression vector) cells are labeled by red fluorescent protein mCherry, and single mCherry-labeled Ad-M3C-infected cell is sorted by FACS (fluorescence-activated cell sorting) for single-cell RNA sequencing (scRNA-seq) library construction. The diagram is created with BioRender. (B) Uniform manifold approximation and projection (UMAP) plot of 2641 single cells colored by labels of unsupervised clustering. The cells are collected from predetermined time points during the process of in vivo transdifferentiation. (C) UMAP plot of 2641 single cells highlighted by the expression of acinar cell marker gene *Cpa1* and β cell marker gene *Ins2*. log-NC, log-normalized count. (D) The expression level of key markers in each cluster. Clusters labeled in blue include cells involved in the transdifferentiation route from acinar cells to induced β cells. (E) Bar plot of gene ontology (GO) terms enriched by up-regulated genes of cluster F (acinar cells, the origin of transdifferentiation) and cluster I. SRP, signal recognition particle; ER, endoplasmic reticulum. (F) Immunostaining of insulin (β cell marker) at different time points during the process of transdifferentiation. Scale bars, 25 μ m. DAPI, 4',6-diamidino-2-phenylindole.



fates. Since the cell trajectory bifurcated at C5 and extended into two branches, we systematically analyzed the transcriptome differences between C5 cells belonging to lineage 1 and lineage 2. The results showed that key marker genes (*Ins2*, *G6pc2*, and *Slc2a2*) of β cell were expressed higher in C5 cells belonging to lineage 1, and up-regulated genes in these cells were associated with typical β cell functions (fig. S2, C and D), indicating the existence of

transcriptomic heterogeneity within C5 cells. These results demonstrated that all the reprogramming cells went through a common linear branch in the early stage from C1 to C4 and bifurcated into two branches in C5, which may lead to two different ends in the later stage. We defined the common part (C1 to C4) of both lineage 1 and lineage 2 as stage 1 and the bifurcated part of the

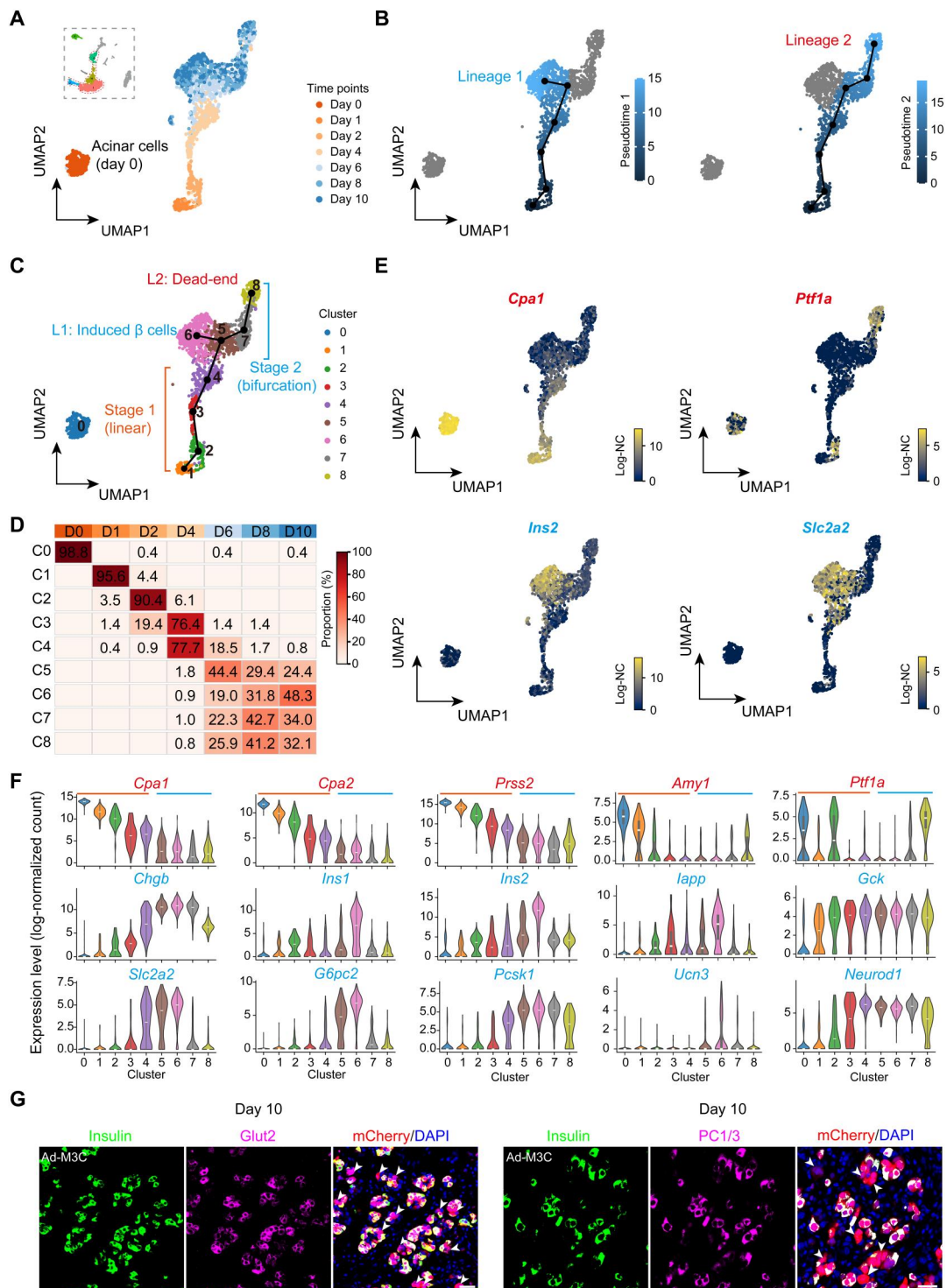


Fig. 2. Constructed cell trajectory uncovers two distinct stages along the process of in vivo transdifferentiation. (A) UMAP plot of 1855 retained cells. Each dot represents a single cell colored by time point. (B) UMAP plot with inferred lineage structure. Each dot represents a single cell colored by estimated pseudotime for lineage 1 (left panel) and lineage 2 (right panel). (C) UMAP plot of retained 1855 reprogramming cells with constructed cell trajectory, which consists of two lineages. Each dot represents a single cell colored by cluster. L1, lineage 1; L2, lineage 2. (D) Percentage of cells at each time point in each cluster. The sum of each row is 100. D, day. (E) UMAP plot showing the expression pattern of key marker genes of acinar cells (labeled in red) and β cells (labeled in blue). (F) Violin plots showing the expression patterns of key marker genes of acinar cells (labeled in red) and β cells (labeled in blue). (G) Coimmunostaining of insulin with Glut2 (encoding by *Slc2a2*) or PC1/3 (encoding by *Pcsk1*) at day 10 of M3 factors induced in vivo transdifferentiation. The white arrowheads point to the reprogramming cells at the state of the dead end. Scale bars, 25 μ m.

trajectory (C5, C6, C7, and C8) as stage 2 of the transdifferentiation process (Fig. 2C).

To roughly infer the cell type of C6 and C8, which were the end points of two lineages, we checked the expression trend of several canonical markers of the acinar cell, duct cell, β cell, progenitor cell, and other pancreatic endocrine cells along these two lineages. We found that the expression of most acinar marker genes, including *Cpa1*, *Cpa2*, *Prss2*, *Amy1*, and *Muc1*, decreased from C0 to C5 and further to C6 or to C7 and C8, while the acinar cell marker *Ptf1a* was expressed highly in C8 (Fig. 2, E and F, and fig. S2E). Meanwhile, the expression of endocrine cell marker gene (*Chgb*) and other key β cell marker genes (*Ins1*, *Ins2*, *Iapp*, *Gck*, *Slc2a2*, *G6pc2*, *Pcsk1*, *Ucn3*, and *Neurod1*) increased gradually from C0 to C6 (Fig. 2, E and F, and fig. S2E), and heterogeneous expression of the above β cell marker genes were detected from C5 to C8 (Fig. 2F). These β cell marker genes were highly expressed in C6, and most had distinguishable lower expression in C8. In addition, we found that the expression of duct cell markers (*Sox9* and *Krt19*), progenitor cell marker (*Cd34*), and non- β endocrine cell markers (*Gcg*, *Sst*, *Ppy*, and *Ghrl*) were also low in C6. On the contrary, *Ghrl*, *Krt19*, *Muc1*, *Cpa1*, *Cpa2*, *Prss2*, and *Amy1* were highly expressed in C8 compared to C6 (Fig. 2F and fig. S2E). It seems that C6 cells had a better expression of β cell markers, while C8 cells exhibited a variety of molecular characteristics and did not have a firm preference for a certain cell type. Furthermore, we systematically analyzed the cell percentage of each cluster at the indicated time points. We found that the C6 cells (induced β cells) first emerged on day 4, and only the cell percentage of C6 at each time point gradually increased from day 4 to 10 (fig. S2F). On the basis of the above features of C6 and C8, we inferred C6 as the successfully induced β cells and C8 as the dead-end state (failed reprogramming).

Besides, the results of quantitative real-time polymerase chain reaction (qPCR) further confirmed the decreased expression of acinar cell marker genes (*Cpa1*, *Cpa2*, and *Prss2*) from day 0 to 4 and up-regulated expression of *Ins2* after day 4 (fig. S2G). Moreover, the coimmunostaining for insulin with glucose transporter type 2 (*Glut2*) (encoding by *Slc2a2*) and insulin with proprotein convertase 1/3 (*PC1/3*) (encoding by *Pcsk1*) on day 10 indicated the existence of successful and failed reprogrammed cells (Fig. 2G). Together, through single-cell transcriptomic analysis, we unveiled two different stages during the process of in vivo transdifferentiation from adult acinar cells to induced β cells. However, the underlying molecular regulators remain to be further dissected.

M3 factors induced *p53* acts as a barrier in the initial stage of in vivo transdifferentiation

To identify the potential regulators of cell fate conversion, we performed a deeper analysis of transcriptomic changes in stage 1 and stage 2, respectively. First, we compared the transcriptome of cells in C1 and C0 to detect the molecular changes and identify key regulators in the early stage of transdifferentiation, and the differential expression analysis generated a large number of differentially expressed genes (DEGs; 1014 up-regulated and 673 down-regulated genes in C1), many of which were particularly significant (Fig. 3A). To narrow the research scope, we performed functional enrichment analysis for these up-regulated genes in C1 and found that several GO terms related to cell cycle regulation were enriched with high significance (Fig. 3B). In addition, we also detected potential regulators of those up-regulated genes in C1 and noticed that *Trp53* (a

well-known regulator of cell cycle arrest) was the second most significantly enriched TF (Fig. 3C). On the basis of these findings, we checked the statistical significance of the differential expression of *Trp53*, which was very high [false discovery rate (FDR) = 1.88×10^{-19}] (fig. S3A). Furthermore, *Cdkn1a* (*p21*), a well-studied direct transcriptional target of *Trp53* that controlled cell cycle progression, was also significantly (FDR = 7.72×10^{-23}) up-regulated in C1, while *Mki67* (a marker of cellular proliferation) was almost not expressed during the whole transdifferentiation process (fig. S3A). Collectively, the expression of *Trp53* was activated in C1, and it was likely to be one of the central regulators of transcriptomic change in C1, suggesting that *Trp53* might play an important role in the early stage of transdifferentiation. Above all, we focused on *Trp53* for further experimental verification.

To verify the existence of cell cycle arrest in the early stage, we detected the cell proportion of $\text{Ki67}^+\text{mCherry}^+$ in the pancreas that was infected with Ad-M3C (adenovirus expressing M3 factors and mCherry) and Ad-mCherry (only expressing mCherry for control) on day 4, respectively. The result showed that Ki67 was completely suppressed in M3-expressed reprogrammed cells (fig. S3B), suggesting that the cell cycle arrest occurred in the reprogramming cells. In addition, we found that the up-regulation of *p53* and *p21* on day 4 was induced by M3 factors (Fig. 3D). Further analysis revealed that the up-regulation of *p21* depended on *p53* for the cell proportion of $\text{p21}^+\text{mCherry}^+$ cells in *p53* knockout *Rag1*^{-/-} (*Rag1*^{-/-} *p53*^{-/-}) mice that decreased significantly on day 4 (fig. S3C). Furthermore, we found that cell proliferation was partly recovered in M3-expressed reprogramming cells from *Rag1*^{-/-} *p53*^{-/-} mice on day 4 (fig. S3B). Consistently, the results of qPCR also revealed that *p53* was transiently up-regulated in the early stage, suggesting that *p53* may play a vital role during stage 1 of in vivo transdifferentiation (fig. S3D).

On the basis of the above results, we tried to dissect the role of *p53* for β cell regeneration induced by M3 factors in *Rag1*^{-/-} *p53*^{-/-} mice on day 4 and 10 (Fig. 3E). We found that the deletion of *p53* significantly increased the proportion of newly regenerated insulin-positive cells both on day 4 and 10 (Fig. 3F). Collectively, we illustrated that *p53* acts as a reprogramming barrier that hinders the M3 factor-induced β cell regeneration through arresting cell cycle in the early stage.

High expression of *Dnmt3a* drives transdifferentiation into the dead-end state

Furthermore, we want to investigate the potential factor that regulates the cell fate establishment of induced β cells. According to the illustration of previous work, remodeling of DNA methylation occurs within day 10 during the process of in vivo transdifferentiation from acinar cells to β cells (14), indicating that the epigenetic modification may be responsible for the transdifferentiation. However, the underlying regulatory mechanisms of DNA methylation are still unknown.

We compared the transcriptome between cells of the two end points of transdifferentiation (C6, induced β cells and C8, dead end) and found that *Dnmt3a* (FDR = 2.88×10^{-5}) was significantly up-regulated in C8 (dead-end) in the comparison with C6 (induced β cells) (Fig. 4A). Functional enrichment revealed that *Dnmt3a* involved GO terms, "DNA methylation or demethylation," and gene expression silencing-associated GO terms were significantly enriched in C8 up-regulated genes (Fig. 4B). These results

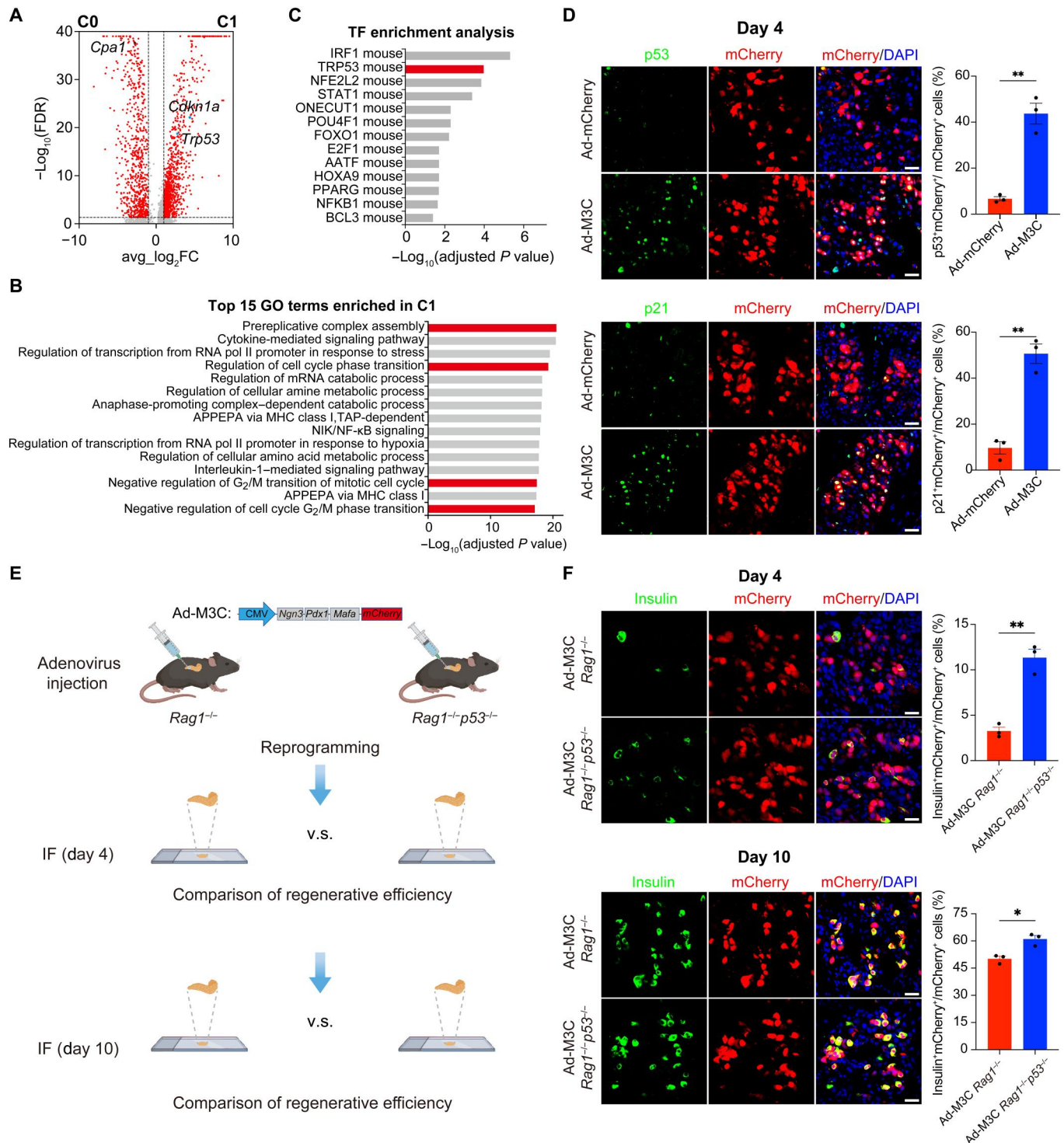


Fig. 3. M3 factors induced p53 acts as an early barrier in stage 1 of transdifferentiation. (A) Volcano plot of differential expression analysis between C0 and C1. Each dot represents a gene, and differentially expressed genes (DEGs) are highlighted in red. FDR, false discovery rate; FC, fold change. See also table S2. (B) Bar plot of significantly enriched GO terms of up-regulated genes in C1 cells with the cell cycle regulation-associated GO terms highlighted in red. APPEPA, antigen processing and presentation of exogenous peptide antigen; NIK, NF- κ B-inducing kinase; NF- κ B, nuclear factor; MHC, major histocompatibility complex. TAP, Transporter associated with antigen processing. (C) Bar plot of significantly enriched transcription factors (TFs) of up-regulated genes in C1 cells. The significance cutoff is set as adjusted $P \leq 0.05$. (D) Comparison of p53⁺mCherry⁺ or p21⁺mCherry⁺ in adenovirus-infected (Ad-mCherry and Ad-M3C) pancreatic cells at day 4 in vivo. Scale bars, 25 μm . (E) Schematic diagram of experiment design. IF, immunofluorescence. The diagram is created with BioRender. (F) Efficiency comparison of M3-induced β cell regeneration in *Rag1*^{-/-} and *Rag1*^{-/-p53}^{-/-} mice on days 4 and 10. Scale bars, 25 μm . Results of bar plot are presented as means \pm SEM; * $P \leq 0.05$; ** $P \leq 0.01$, two-sample t test, $n = 3$ mice.

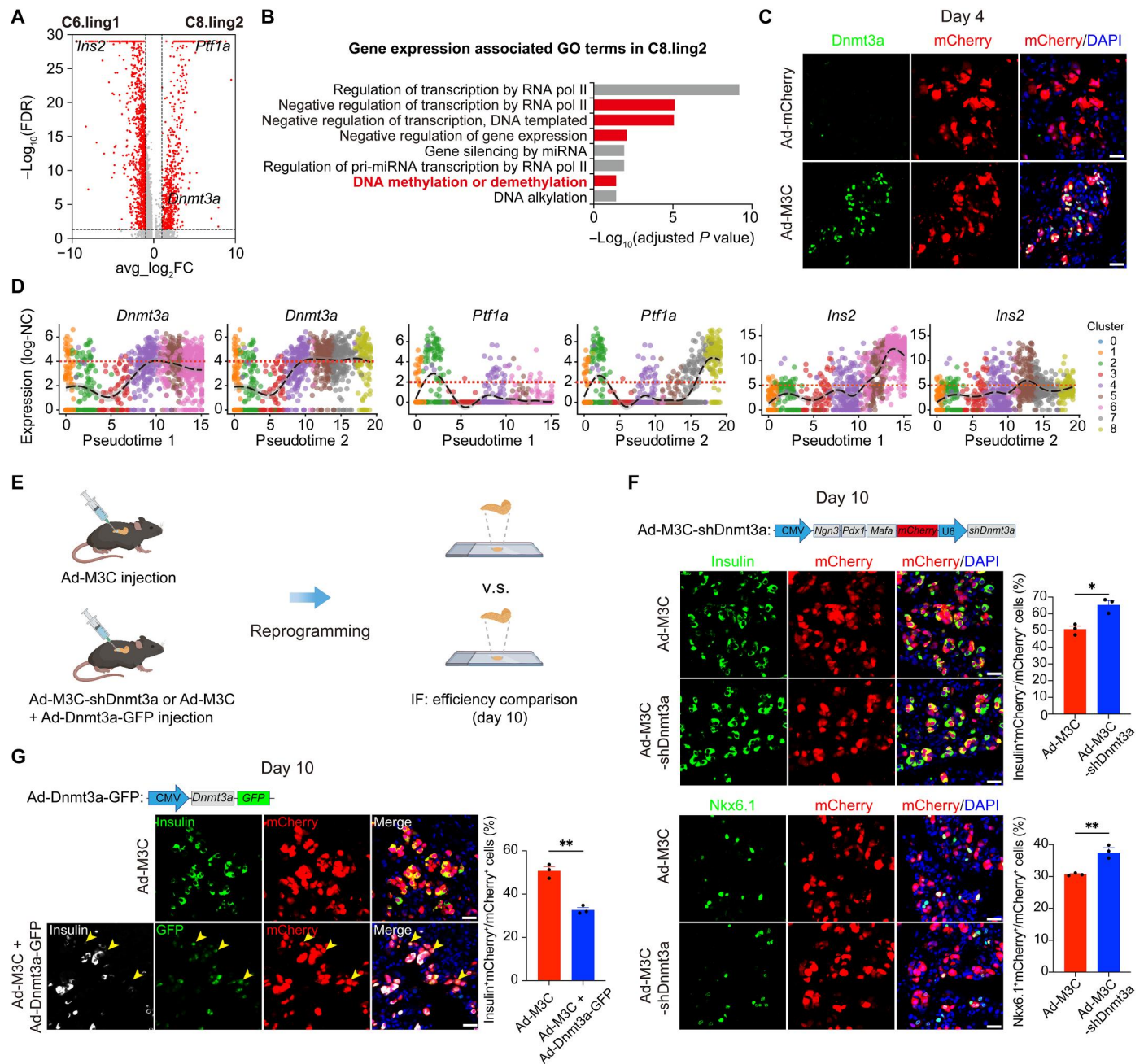


Fig. 4. High expression of *Dnmt3a* effectively drives cells toward to the dead end of transdifferentiation in vivo. (A) Volcano plot of differential expression analysis between two clusters of the end of lineage 1 (C6) and lineage 2 (C8). The DEGs are shown in table S3. (B) Bar plot of several picked GO terms significantly enriched by up-regulated genes in C8 (the dead end). These GO terms are associated with gene expression regulation and are *Dnmt3a* involved. miRNA, microRNA. (C) Detection of *Dnmt3a* in the pancreas of Ad-mCherry- and Ad-M3C-infected pancreas through immunostaining in vivo. Scale bars, 25 μm . (D) Expression trend of *Dnmt3a* (candidate regulator), *Ptf1a* (a marker gene of C8, the dead end), and *Ins2* (a marker gene of C6, induced β cells) over pseudotime of lineage 1 (toward to induced β cells) and lineage 2 (toward to the dead end). Each dot represents a single cell, and cells are colored by cluster information. (E) Schematic of *Dnmt3a* knockdown experiment. The diagram is created with BioRender. (F) Comparison of the proportion of Insulin⁺mCherry⁺ and Nkx6.1⁺mCherry⁺ cells in Ad-M3C and Ad-M3C-shDnmt3a-infected pancreatic cells in vivo. Results of bar plot are presented as means \pm SEM; * $P \leq 0.05$; ** $P \leq 0.01$, two-sample t test, $n = 3$ mice. Scale bars, 25 μm . (G) Comparison of the proportion of Insulin⁺mCherry⁺ cells in Ad-M3C and Ad-M3C + *Dnmt3a*-GFP-infected pancreatic cells in vivo. The yellow arrowheads point to cells that have strong signal of *Dnmt3a* and no signal of insulin. Results of the bar plot are presented as means \pm SEM; ** $P \leq 0.01$, two-sample t test, $n = 3$ mice. Scale bars, 25 μm .

demonstrated that *Dnmt3a* may play a crucial role in the formation of bifurcation of cell trajectory.

Thereafter, we performed a further systematic investigation of *Dnmt3a* during the whole process of in vivo transdifferentiation. Through the expression pattern of *Dnmt3a* in each cluster during the transdifferentiation, we found that *Dnmt3a* was already up-regulated in C4 (mainly contained cells from day 4) (fig. S4A). However, the other two DNA methyltransferase encoding genes *Dnmt1* and *Dnmt3b* were found lowly expressed during the whole process (fig. S4A). Immunostaining showed that M3 factors induced the up-regulation of *Dnmt3a* on day 4 (Fig. 4C). In addition, the heterogeneous expression of *Dnmt3a* was uncovered in the bifurcated stage 2 (C5, C6, C7, and C8) (fig. S4A). From C5 to C6,

the expression of *Dnmt3a* decreased and thus exhibited a moderately lower expression level in C6 (the end of the successfully reprogrammed lineage 1). However, from C5 to C7 and further to C8, the expression of *Dnmt3a* continuously elevated and thus exhibited a high expression level in C8 (the end of the failed reprogrammed lineage 2) (Fig. 4D and fig. S4A). Here, we proposed a hypothesis that high expression of *Dnmt3a* may also act as a reprogramming barrier for β cell regeneration during the process of in vivo transdifferentiation.

To validate the hypothesis, we interfered the expression level of *Dnmt3a* by knocking down and overexpressing this gene through adenoviral delivery, respectively. First, we knocked down the expression of *Dnmt3a* using short hairpin RNA. A tandem expression

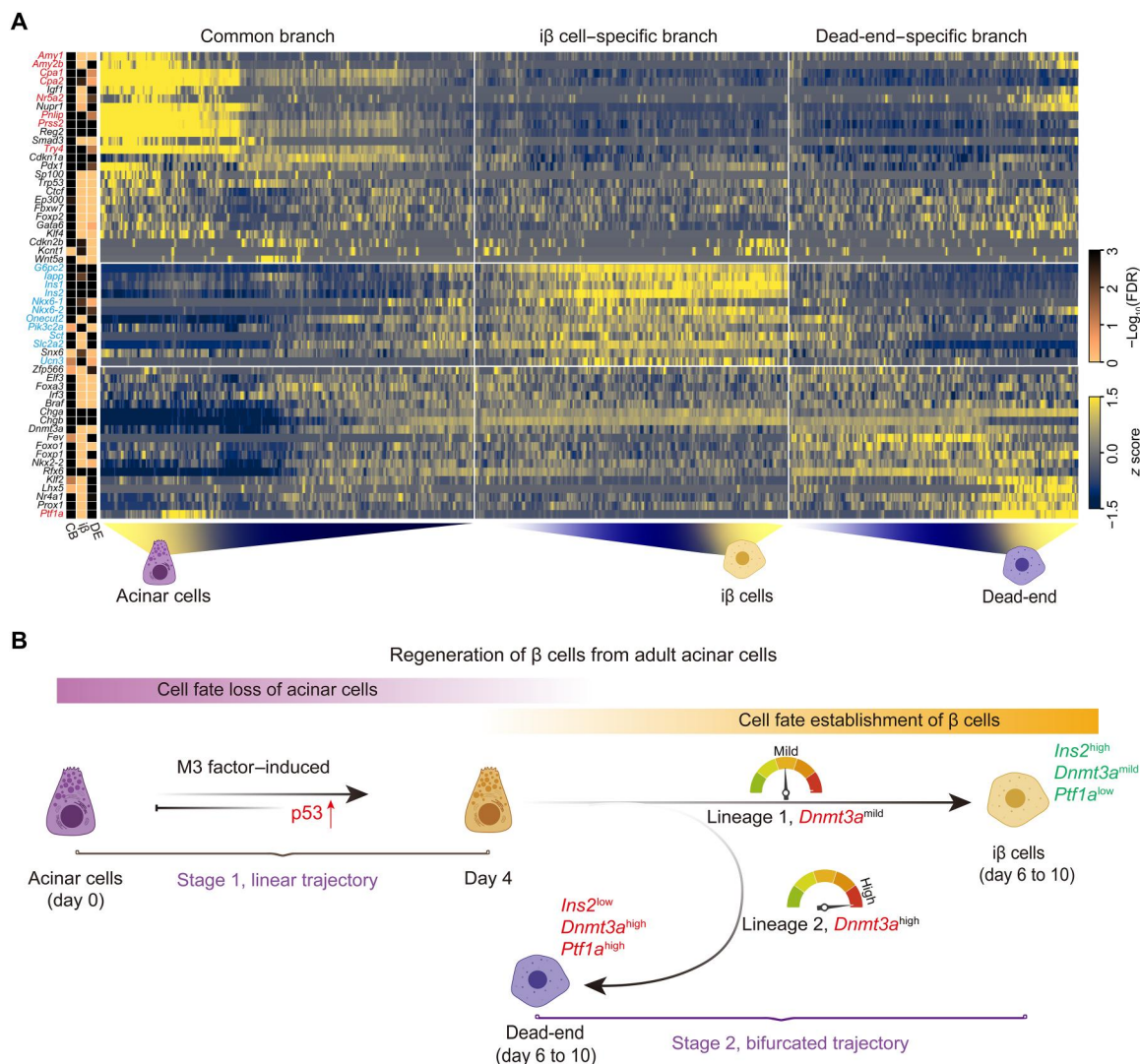


Fig. 5. Molecular and cellular roadmap of in vivo transdifferentiation from acinar cells to $i\beta$ cells. (A) The heatmap of temporally dynamic genes along the trajectory of common branch, induced β ($i\beta$) cell-specific branch, and dead-end-specific branch. The acinar cell marker genes are labeled in red, and the β cell marker genes are labeled in blue. CB, common branch; DE, dead end. (B) The working hypothesis for reprogramming barrier factors during M3 factor-induced transdifferentiation from acinar cells to $i\beta$ cells in vivo. The *p53* transiently up-regulated in stage 1 and acts as a reprogramming barrier. In stage 2, heterogeneous expression of *Dnmt3a* may lead to bifurcation of cell fate. Mild expression of *Dnmt3a* converts reprogramming cells into β cells, and high expression of *Dnmt3a* drives cells toward to a dead-end state of reprogramming. The cells of dead-end show high expression of *Ptf1a* (acinar cell marker gene), *Dnmt3a*, and low expression of *Ins2* (β marker gene). The diagram is created with BioRender.

vector that shDnmt3a coexpressed with M3 factors was constructed to increase the knockdown efficiency (Fig. 4E). The immunostaining showed reduced level of *Dnmt3a*, which proved that shDnmt3a was effective on day 4 (fig. S4B). Moreover, we found that the knockdown of *Dnmt3a* significantly increased the cell proportion of Insulin⁺ and Nkx6.1⁺ cells in M3 factors expressing cells (mCherry labeled) (Fig. 4F). These results demonstrated that the suppression of *Dnmt3a* could improve the regenerative efficiency of β cells in vivo. On the contrary, the overexpression of *Dnmt3a* together with M3 factors effectively reduced the cell proportion of Insulin⁺mCherry⁺ cells (Fig. 4G). Together, we demonstrated that high expression of *Dnmt3a* plays a reprogramming barrier role during the process of in vivo transdifferentiation from acinar cells to β cells.

DISCUSSION

Although the regenerative capacity of adult mammalian cells is limited, the in vivo transdifferentiation of pancreatic β cells from adult mouse acinar cells provides an ideal model to study regeneration in mammals. Nevertheless, there is still a lack of understanding of this regenerative process. Here, we apply single-cell transcriptomic technology to dissect the cellular and molecular dynamic roadmap of in vivo transdifferentiation, which is induced by M3 factors. By analyzing the global transcriptomic changes during the in vivo transdifferentiation process, we reveal that the cell trajectory of transdifferentiation can be seemed as two stages. In the early stage, all cells follow the same branch, which is common to lineage 1 and 2, and exhibit gradually reduced expression of acinar cell marker genes, such as *Cpa1*, *Cpa2*, *Amy1*, *Amy2b*, *Nr5a2*, *Pnlip*, *Prss2*, and *Try4*, and increased expression of β cell marker genes, such as *G6pc2*, *Iapp*, *Ins1*, *Ins2*, *Nkx6.1*, *Nkx6.2*, *Onecut2*, *Slc2a2*, and *Ucn3*. In addition, the later stage is characterized by the trajectory bifurcating into two branches, one of which corresponds to the cell fate of successful regeneration, named as the induced β cell specific branch, and the other corresponds to the cell fate of failed reprogramming, named as the dead-end-specific branch. These two branches exhibit heterogeneous gene expression patterns. Generally, the expression of β cell marker genes continues to increase and remain stable along the induced β cell-specific branch but decreases and keeps a low level along the dead-end-specific branch. Furthermore, several acinar cell marker genes including *Ptf1a*, *Amy2b*, and *Nr5a2* are reactivated in the dead-end-specific branch, which is not observed in the induced β cell-specific branch (Fig. 5A).

Combining the published scRNA-seq dataset (21), we also attempt to score each cell using signatures of unperturbed endogenous adult acinar cells and β cells to evaluate the relative changes in cell transcriptome profiles during the transdifferentiation process, in which cells gradually lose acinar cell signatures and acquire β cell signatures (details see the Supplementary Text and fig. S5). As expected, the score of transdifferentiation is lowest in C0 and gradually increases along the path from C1 to C5. Then, on the one hand, the score continues to rise from C5 to C6 along lineage 1 and lastly is the highest in C6. While on the other hand, the score falls back from C5 to C7 and further to C8 along lineage 2 and lastly is lower than C6 in C8 (fig. S5, B and C). These results indicate that C6 cells have more β cell and less acinar cell signature genes than C8

cells (fig. S5D), supporting the two lineages corresponding to different cell fates identified through our data.

Moreover, through functional analysis, we identify that *p53* is significantly up-regulated in the initial stage and acts as a barrier for β cell regeneration. In addition, the DNA methyltransferase encoding gene *Dnmt3a* is identified as another reprogramming barrier during the process of in vivo transdifferentiation. High expression of *Dnmt3a* represses β cell regeneration, and knockdown of *Dnmt3a* through short hairpin RNA could effectively increase the efficiency of β cell regeneration (Fig. 5B). Above all, we decipher a high-resolution molecular roadmap of in vivo β cell regeneration and identify two key barrier factors during the transdifferentiation from adult acinar cells to β cells.

On the basis of the high-resolution molecular roadmap of transdifferentiation from adult acinar cells to induced β cells, we have a deeper understanding of mammalian regeneration. Taking the β cell regeneration as an example, the regeneration of β cells via direct reprogramming has made great progress in the past decades. It has been reported that β cells could be transdifferentiated from nonpancreatic and pancreatic cells, such as stomach cells, intestinal cells, pancreatic exocrine cells, and islet α cells (6, 22–25). All the above regenerated β cells are triggered by the coexpression of M3 factors. In addition, it has been well established that cellular reprogramming is characterized by the existence of barriers that block the process. For instance, *Ptbp1* and *Bmi1* are identified as barriers during the conversion of fibroblasts into induced cardiomyocytes (11, 26). Besides, in several somatic cell reprogramming and direct reprogramming cases (iPSCs and neurons) that are induced by defined factors, *p53*-dependent cell cycle arrest is identified as a barrier for the cell fate conversion (27–30). In line with the above studies, we also illuminate that *p53* serves as a barrier in the initial stage of β cell regeneration. It seems that *p53* may be a common barrier for mammalian cell regeneration. On the basis of this notion, *p53* may also act as a barrier during the cell fate conversion of stomach cells and intestinal cells into β cells, which remains to be further explored. Collectively, *p53* may be a common target for facilitating adult mammalian cell regeneration.

Meanwhile, the mechanism for the dead-end formation during the in vivo transdifferentiation from adult acinar cells to β cells will need further analysis. As we mentioned above, the *Ptf1a* is specifically up-regulated in the dead end. On the other hand, we find that *Ptf1a* is transiently up-regulated at the early time of the initial stage with mild expression level (Figs. 4D and 5A). The heterogeneous expressions of *Ptf1a* at different stages of the reprogramming process may have different effects on transdifferentiation. According to previous studies, *Ptf1a* is a critical TF for the development of the pancreas and serves as an identity maintainer of adult acinar cells (31, 32). In the developing pancreas, *Ptf1a* has a dual effect in which high expression of *Ptf1a* promotes exocrine cell development but suppresses endocrine cell development. However, low expression of *Ptf1a* promotes endocrine cell development (33). Consistently, our results also reveal the dynamic expressions of *Ptf1a* in β cell fate establishment from adult acinar cells. In addition, the vary of transgenic (*Ngn3*, *Pdx1*, and *Mafa*) expression levels may also contribute to the formation of dead-end states. Perhaps the lower expression of M3 factors could not trigger or complete the cell fate conversion of acinar cells in some stages of transdifferentiation, thereby leading to a set of acinar cell marker genes that were still partly up-regulated at the end of transdifferentiation. The

relationship between transgenic expression level and reprogramming efficiency will need further evaluation.

Furthermore, we have confirmed that the formation of a dead end is associated with high expression of *Dnmt3a* during the later stage of transdifferentiation from acinar cells to β cells. A moderate expression of *Dnmt3a* might be essential for successful β cell regeneration, because the up-regulation of *Dnmt3a* in the early stage is observed upon activation by M3 factors, and the β cell fate is inhibited in cells with high expression of *Dnmt3a* (dead-end). Moreover, when *Dnmt3a* is overexpressed, the regenerative efficiency of β cells from acinar cells is significantly suppressed. Vice versa, when *Dnmt3a* is knocked down, the regenerative efficiency is markedly increased. It is well known that *Dnmt3a* is a vital de novo methyltransferase that establishes DNA methylation patterns during the process of embryonic development and somatic cell reprogramming (34–36). Knockout of *Dnmt3a* in embryonic stem cells results in failed differentiation (37). These studies suggest that systematic epigenetic remodeling is essential for successful cell fate determination. However, the precise role of *Dnmt3a* in the process of transdifferentiation from acinar cells to induced β cells needs further exploration. In total, we chart a high-resolution regenerative roadmap of in vivo transdifferentiation from adult mouse acinar cells to induced β cells. This roadmap will provide new insights into the understanding of mammalian cell regeneration by in vivo reprogramming method.

MATERIALS AND METHODS

Animals and surgery

All the mice were housed under specific pathogen-free conditions at Tongji University, Shanghai, China. The *Rag1*^{-/-} (C57BL/6JSmoc-*Rag1*^{em1Smoc}) mice were purchased from Shanghai Model Organisms Center Inc. The *p53*^{-/-} (C57BL/6-*Trp53*^{tm1/Bcgen}) mice were purchased from Biocytogen Pharmaceuticals (Beijing) Co. Ltd. (cat. no. 110167). *Rag1*^{-/-} mice were crossed with *p53*^{-/-} mice to generate double-knockout mice. Adult male or female mice (6 to 12 weeks old) were selected for adenovirus injection at the tail of pancreas. Each mouse was injected with 100 μ l of adenovirus [2×10^{10} plaque-forming units (PFU)/ml] as previously described (14). All the experiments on mice were approved by Tongji University Animal Research Committee (TJAB03620102).

Adenoviral production

Vector construction of interest genes was performed as previously described (6, 14). The coding sequencing of target genes were first cloned into a shuttle vector that contains 2A-mCherry or 2A-EGFP by using ClonExpress Ultra One Step Cloning Kit (Vazyme, C115-01). The primers for gene clone and vector construction are listed in table S1. High-titer ($>2 \times 10^{11}$ PFU/ml) adenovirus were produced according to the manufacturer's instructions of Vivapure Adenopack purification kit (Sartorius, VS-AVPQ022). More details about the above procedures could refer to published protocol (DOI: 10.1007/978-1-4939-0512-6_17) (38). The pAd-M3C has been deposited at Addgene (Addgene, plasmid no. 61041). The complete DNA sequence of the pAd-M3C vector and the sequence of the main context of other vectors are provided in the Supplementary Materials (data S1).

Immunostaining assay

The adult pancreas injected with adenovirus was dissected and fixed with 4% paraformaldehyde on ice for 1 hour on the decolorizing shaker at the rotating speed of 50 revolutions per minute. Then, the tissue was washed with ice-cold Dulbecco's Phosphate-Buffered Saline (DBPS) twice and treated with 30% sucrose solution overnight to dehydrate the tissue. Pancreas was embedded with an optimal cutting temperature compound and frozen at -80°C . The frozen tissue was cut into 10- μ m sections using a cryostat at -20°C (Leica).

The tissue section was blocked with phosphate-buffered saline (PBS) solution containing 0.1% Triton X-100 and 5% donkey serum for 1 hour at room temperature. The primary antibody was incubated at 4°C overnight, and the tissue sections were washed with PBST (PBS containing 0.1% Triton X-100) solution three times before incubating with the second antibody. The incubation of the secondary antibody was performed at room temperature for 1 hour. The primary antibodies were listed as follows: mouse anti-insulin (1:1000; Sigma-Aldrich, I2018), goat anti-Glut2 (1:200; Santa Cruz Biotechnology, sc-7580), mouse anti-p53 (1:200; Cell Signaling Technology, 2524), rabbit anti-Dnmt3a (1:200; Cell Signaling Technology, 3598s), rabbit anti-Ki67 (1:100; Neomarkers, RM-9106-S0), rabbit anti-p21 (1:200; Abcam, ab188224), and rabbit anti-PC1/3 (1:200; Millipore, AB10553). Alexa Fluor 488 and Alexa Fluor 647 affinity donkey secondary antibodies were purchased from the Jackson ImmunoResearch. Immunofluorescence pictures were captured by using Leica SP8 confocal microscope.

Preparation of single-cell and sequencing library construction

Adenovirus-infected pancreas ($n = 3$ biological replications) were perfused with 2 to 3 ml of collagenase P (0.8 mg/ml; Roche, 11213873001) through the common bile duct and digested at 37°C for 15 to 20 min. Digestion was stopped by adding 15 to 20 ml of Dulbecco's modified Eagle's medium containing 10% fetal bovine serum (FBS), 1% PenStrep, and 1% Hepes (quenching buffer). The suspension was filtered with a 70- μ m-cell strainer to exclude the islets. The filtrate was spun for 3 min at 300g, 4°C , and the pellet was resuspended with ice-cold DPBS to clear FBS twice. The pellet was dissociated into single cells using 1 ml of TrypLE Express (Gibco, 12604021) at 37°C for 15 to 20 min, and the solution was mixed up and down gently by P1000 pipette during the digestion process to improve the proportion of single cells. After digestion, the cell suspension was spun for 3 min at 300g, 4°C , resuspended with FACS buffer (DPBS with 0.5% BSA), and filtered with a 40- μ m strainer to obtain single-cell suspension. The high viability single cells were labeled by Calcein Blue AM (1 mg/ml; Invitrogen, C1429), which was added into cell suspension directly at the ratio of 1:2000. The single cells labeled by mCherry and Calcein Blue AM were sorted into cell lysis buffer in 96-well plates through MoFlo Astrios four lasers flow cytometry. The collected samples were flash-frozen at the mixture of dry ice and absolute ethanol.

The isolation of pancreatic exocrine cells, including acinar cells (defined as day 0), of no adenovirus injected mice were also processed as above procedures. The Calcein Blue AM-labeled (1 mg/ml; 1:2000) high viability single exocrine cells were sorted into 96-well plates and flash-frozen as above description.

The scRNA-seq libraries were constructed according to a modified Smart-seq2 protocol. The detail procedures were performed as in the previous description (DOI: 10.1016/j.gpb.2021.07.004) (39).

Quantitative real-time PCR

Adenovirus infected cells were purified by FACS. Total RNA was extracted using GenElute Single Cell RNA Purification Kit (Sigma-Aldrich, RNB300) and reverse transcribed according to the instructions of the kit. Real-time PCR was carried out by using SuperReal PreMix Plus (SYBR Green) (TIANGEN, EP205). *Sdha* was used as an internal control. Relative gene expression was calculated using the formula of $2^{-\Delta\Delta ct}$. The primers of target genes are listed in table S1.

scRNA-seq data processing and downstream analysis

Processing sequencing reads to UMI counts

Read processing was performed as previously described (39). Unique molecular identifier (UMI) count data from all cells were merged into one single matrix, which included the metadata information of each cell such as cell collection date, transdifferentiation time point, etc. Cells were selected for further analysis if they had at least 1000 detected genes (with UMI count >1; fig. S1A). Genes were retained if they were detected in at least 10 cells. These rules resulted in a UMI count matrix with 2641 valid cells and 15,143 detected genes.

Normalization of UMI counts

Normalization is required to eliminate cell-specific biases before downstream quantitative analyses. We used *scran* (40, 41) that pools counts from many cells to increase the count size for accurate size factor estimation to overcome the problem due to the dominance of low and zero counts in scRNA-seq data. The estimated size factors were used to calculate normalized expression values.

Clustering cells and filtering clusters that are not in the transdifferentiation route

After normalization, log-transformed normalized counts were used to cluster cells using the R package *Seurat* v3 (42). The default "Variance-stabilizing transformation (vst)" method was used to find variable genes as features before running a principal components analysis (PCA) for further dimensionality reduction. We selected the top 15 PCs as input to construct the shared nearest neighbor (SNN) graph and then determine cell clusters by optimizing the modularity function, which roughly grouped the cells into 10 clusters. Besides, the top 15 PCs were also used as input to run the UMAP, a nonlinear dimensional reduction method for visualization. Then, by comparing every cell cluster to all the other cells using Wilcoxon rank sum test, the marker genes of each cluster were identified by using adjusted $P \leq 0.05$ and $\log_2(\text{fold change}) > 0.25$ as cutoffs. Functional enrichment analyses of these marker genes were performed using R package *enrichR* (<https://CRAN.R-project.org/package=enrichR>), and GO terms (<http://geneontology.org/>) served as the gene sets to be queried. According to the marker genes and the functional enrichment results of each cluster, only clusters (clusters F to J) related to the biological processes that we focus on were retained for further analysis (Fig. 1, B and D).

Reclustering cells

To better characterize the 1855 retained cells, we reapplied the vst method to their transcriptomes to find variable features, and then PCA, UMAP, and clustering analyses were carried out again using the same methods as mentioned above. The cells were separated into 10 clusters (C0 to C9) and those in the smallest cluster (C9) were filtered out as outliers.

Cell lineage and pseudotime inference

We identified lineage structure for cells in a continuous process of transdifferentiation (C1 to C8) by *Slingshot*, which infers cell lineage by fitting a minimum spanning tree on the clusters and estimates the underlying cell-level pseudotime for each lineage by their new method called simultaneous principal curves (20). Next, we identified temporally expressed genes (i.e., whose expression is changing in a continuous manner over pseudotime) by *tradeSeq*, which fits a general additive model using a negative binomial noise distribution for each gene to model the relationship between gene expression and pseudotime (43).

Differential expression analysis and enrichment analysis

DEGs between two cell clusters were detected by Wilcoxon rank sum test with adjusted $P \leq 0.05$ and $|\log_2\text{-fold change}| > 1$ as cutoffs. GO terms and TFs enriched by the DEGs were identified by *enrichR* (with adjusted $P \leq 0.05$). The regulatory interactions (TF-target) were obtained from the Transcriptional regulatory relationships unraveled by sentence-based text mining (TRRUST) database (44).

Supplementary Materials

This PDF file includes:

Supplementary Text
Figs. S1 to S5
Table S1
Legends for tables S2 and S3
Data S1

Other Supplementary Material for this manuscript includes the following:

Tables S2 and S3

[View/request a protocol for this paper from Bio-protocol.](#)

REFERENCES AND NOTES

1. K. Takahashi, Cellular reprogramming. *Cold Spring Harb. Perspect. Biol.* **6**, a018606 (2014).
2. H. Wang, Y. Yang, J. Liu, L. Qian, Direct cell reprogramming: Approaches, mechanisms and progress. *Nat. Rev. Mol. Cell Biol.* **22**, 410–424 (2021).
3. K. Takahashi, K. Tanabe, M. Ohnuki, M. Narita, T. Ichisaka, K. Tomoda, S. Yamanaka, Induction of pluripotent stem cells from adult human fibroblasts by defined factors. *Cell* **131**, 861–872 (2007).
4. M. Ieda, J. D. Fu, P. Delgado-Olguin, V. Vedantham, Y. Hayashi, B. G. Bruneau, D. Srivastava, Direct reprogramming of fibroblasts into functional cardiomyocytes by defined factors. *Cell* **142**, 375–386 (2010).
5. T. Vierbuchen, A. Ostermeier, Z. P. Pang, Y. Kokubo, T. C. Südhof, M. Wernig, Direct conversion of fibroblasts to functional neurons by defined factors. *Nature* **463**, 1035–1041 (2010).
6. Q. Zhou, J. Brown, A. Kanarek, J. Rajagopal, D. A. Melton, In vivo reprogramming of adult pancreatic exocrine cells to beta-cells. *Nature* **455**, 627–632 (2008).
7. L. Qian, Y. Huang, C. I. Spencer, A. Foley, V. Vedantham, L. Liu, S. J. Conway, J. D. Fu, D. Srivastava, In vivo reprogramming of murine cardiac fibroblasts into induced cardiomyocytes. *Nature* **485**, 593–598 (2012).

8. O. Torper, U. Pfisterer, D. A. Wolf, M. Pereira, S. Lau, J. Jakobsson, A. Björklund, S. Grealish, M. Parmar, Generation of induced neurons via direct conversion in vivo. *Proc. Natl. Acad. Sci. U.S.A.* **110**, 7038–7043 (2013).
9. W. Niu, T. Zang, Y. Zou, S. Fang, D. K. Smith, R. Bachoo, C. L. Zhang, In vivo reprogramming of astrocytes to neuroblasts in the adult brain. *Nat. Cell Biol.* **15**, 1164–1175 (2013).
10. B. A. Biddy, W. Kong, K. Kamimoto, C. Guo, S. E. Wayne, T. Sun, S. A. Morris, Single-cell mapping of lineage and identity in direct reprogramming. *Nature* **564**, 219–224 (2018).
11. Z. Liu, L. Wang, J. D. Welch, H. Ma, Y. Zhou, H. R. Vaseghi, S. Yu, J. B. Wall, S. Alimohamadi, M. Zheng, C. Yin, W. Shen, J. F. Prins, J. Liu, L. Qian, Single-cell transcriptomics reconstructs fate conversion from fibroblast to cardiomyocyte. *Nature* **551**, 100–104 (2017).
12. B. Treutlein, Q. Y. Lee, J. G. Camp, M. Mall, W. Koh, S. A. M. Shariati, S. Sim, N. F. Neff, J. M. Skotheim, M. Wernig, S. R. Quake, Dissecting direct reprogramming from fibroblast to neuron using single-cell RNA-seq. *Nature* **534**, 391–395 (2016).
13. L. Fu, X. Zhu, F. Yi, G. H. Liu, J. C. I. Belmonte, Regenerative medicine: Transdifferentiation in vivo. *Cell Res.* **24**, 141–142 (2014).
14. W. Li, C. Cavelti-Weder, Y. Zhang, K. Clement, S. Donovan, G. Gonzalez, J. Zhu, M. Stemann, K. Xu, T. Hashimoto, T. Yamada, M. Nakanishi, Y. Zhang, S. Zeng, D. Gifford, A. Meissner, G. Weir, Q. Zhou, Long-term persistence and development of induced pancreatic beta cells generated by lineage conversion of acinar cells. *Nat. Biotechnol.* **32**, 1223–1230 (2014).
15. G. C. Weir, S. Bonner-Weir, J. L. Leahy, Islet mass and function in diabetes and transplantation. *Diabetes* **39**, 401–405 (1990).
16. J. M. Forbes, M. E. Cooper, Mechanisms of diabetic complications. *Physiol. Rev.* **93**, 137–188 (2013).
17. S. Y. Tan, J. L. Mei Wong, Y. J. Sim, S. S. Wong, S. A. Mohamed Elhassan, S. H. Tan, G. P. Ling Lim, N. W. Rong Tay, N. C. Annan, S. K. Bhattamisra, M. Candasamy, Type 1 and 2 diabetes mellitus: A review on current treatment approach and gene therapy as potential intervention. *Diabetes Metab. Syndr.* **13**, 364–372 (2019).
18. D. J. Holmes-Walker, T. W. Kay, Long-term effects of islet transplantation. *Curr. Opin. Organ Transplant.* **21**, 497–502 (2016).
19. F. C. Pan, E. D. Bankaitis, D. Boyer, X. Xu, M. van de Castele, M. A. Magnuson, H. Heimberg, C. V. E. Wright, Spatiotemporal patterns of multipotentiality in Ptf1a-expressing cells during pancreas organogenesis and injury-induced facultative restoration. *Development* **140**, 751–764 (2013).
20. K. Street, D. Riso, R. B. Fletcher, D. das, J. Ngai, N. Yosef, E. Purdom, S. Dudoit, Slingshot: Cell lineage and pseudotime inference for single-cell transcriptomics. *BMC Genomics* **19**, 477 (2018).
21. K. Chen, J. Zhang, Y. Huang, X. Tian, Y. Yang, A. Dong, Single-cell RNA-seq transcriptomic landscape of human and mouse islets and pathological alterations of diabetes. *iScience* **25**, 105366 (2022).
22. Y. J. Chen, S. R. Finkbeiner, D. Weinblatt, M. J. Emmett, F. Tameire, M. Yousefi, C. Yang, R. Maehr, Q. Zhou, R. Shemer, Y. Dor, C. Li, J. R. Spence, B. Z. Stanger, De novo formation of insulin-producing “neo- β cell islets” from intestinal crypts. *Cell Rep.* **6**, 1046–1058 (2014).
23. C. Ariyachet, A. Tovaglieri, G. Xiang, J. Lu, M. S. Shah, C. A. Richmond, C. Verbeke, D. A. Melton, B. Z. Stanger, D. Mooney, R. A. Shivdasani, S. Mahony, Q. Xia, D. T. Breault, Q. Zhou, Reprogrammed stomach tissue as a renewable source of functional β cells for blood glucose regulation. *Cell Stem Cell* **18**, 410–421 (2016).
24. X. Xiao, P. Guo, C. Shiota, T. Zhang, G. M. Coudriet, S. Fischbach, K. Prasad, J. Fusco, S. Ramachandran, P. Witkowski, J. D. Piganelli, G. K. Gittes, Endogenous reprogramming of alpha cells into beta cells, induced by viral gene therapy, reverses autoimmune diabetes. *Cell Stem Cell* **22**, 78–90.e4 (2018).
25. W. Li, M. Nakanishi, A. Zumsteg, M. Shear, C. Wright, D. A. Melton, Q. Zhou, In vivo reprogramming of pancreatic acinar cells to three islet endocrine subtypes. *eLife* **3**, e01846 (2014).
26. Y. Zhou, L. Wang, H. R. Vaseghi, Z. Liu, R. Lu, S. Alimohamadi, C. Yin, J. D. Fu, G. G. Wang, J. Liu, L. Qian, Bmi1 is a key epigenetic barrier to direct cardiac reprogramming. *Cell Stem Cell* **18**, 382–395 (2016).
27. H. Jiang, Z. Xu, P. Zhong, Y. Ren, G. Liang, H. A. Schilling, Z. Hu, Y. Zhang, X. Wang, S. Chen, Z. Yan, J. Feng, Cell cycle and p53 gate the direct conversion of human fibroblasts to dopaminergic neurons. *Nat. Commun.* **6**, 10100 (2015).
28. T. Kawamura, J. Suzuki, Y. V. Wang, S. Menendez, L. B. Morera, A. Raya, G. M. Wahl, J. C. I. Belmonte, Linking the p53 tumour suppressor pathway to somatic cell reprogramming. *Nature* **460**, 1140–1144 (2009).
29. L. L. Wang, Z. Su, W. Tai, Y. Zou, X. M. Xu, C. L. Zhang, The p53 pathway controls SOX2-mediated reprogramming in the adult mouse spinal cord. *Cell Rep.* **17**, 891–903 (2016).
30. H. Hong, K. Takahashi, T. Ichisaka, T. Aoi, O. Kanagawa, M. Nakagawa, K. Okita, S. Yamanaka, Suppression of induced pluripotent stem cell generation by the p53-p21 pathway. *Nature* **460**, 1132–1135 (2009).
31. C. Q. Hoang, M. A. Hale, A. C. Azevedo-Pouly, H. P. Elsässer, T. G. Deering, S. G. Willet, F. C. Pan, M. A. Magnuson, C. V. E. Wright, G. H. Swift, R. J. MacDonald, Transcriptional maintenance of pancreatic acinar identity, differentiation, and homeostasis by PTF1A. *Mol. Cell Biol.* **36**, 3033–3047 (2016).
32. A. Krapp, M. Knöfler, B. Ledermann, K. Bürki, C. Berney, N. Zoerkler, O. Hagenbüchle, P. K. Wellauer, The bHLH protein PTF1-p48 is essential for the formation of the exocrine and the correct spatial organization of the endocrine pancreas. *Genes Dev.* **12**, 3752–3763 (1998).
33. P. D. Dong, E. Provost, S. D. Leach, D. Y. Stainier, Graded levels of Ptf1a differentially regulate endocrine and exocrine fates in the developing pancreas. *Genes Dev.* **22**, 1445–1450 (2008).
34. Y. Kato, M. Kaneda, K. Hata, K. Kumaki, M. Hisano, Y. Kohara, M. Okano, E. Li, M. Nozaki, H. Sasaki, Role of the Dnmt3 family in de novo methylation of imprinted and repetitive sequences during male germ cell development in the mouse. *Hum. Mol. Genet.* **16**, 2272–2280 (2007).
35. X. Guo, Q. Liu, G. Wang, S. Zhu, L. Gao, W. Hong, Y. Chen, M. Wu, H. Liu, C. Jiang, J. Kang, microRNA-29b is a novel mediator of Sox2 function in the regulation of somatic cell reprogramming. *Cell Res.* **23**, 142–156 (2013).
36. M. Okano, D. W. Bell, D. A. Haber, E. Li, DNA methyltransferases Dnmt3a and Dnmt3b are essential for de novo methylation and mammalian development. *Cell* **99**, 247–257 (1999).
37. M. Jackson, A. Krassowska, N. Gilbert, T. Chevassut, L. Forrester, J. Ansell, B. Ramsahoye, Severe global DNA hypomethylation blocks differentiation and induces histone hyperacetylation in embryonic stem cells. *Mol. Cell Biol.* **24**, 8862–8871 (2004).
38. C. Cavelti-Weder, W. Li, G. C. Weir, Q. Zhou, Direct lineage conversion of pancreatic exocrine to endocrine beta cells in vivo with defined factors. *Methods Mol. Biol.* **1150**, 247–262 (2014).
39. G. Liu, Y. Li, T. Zhang, M. Li, S. Li, Q. He, S. Liu, M. Xu, T. Xiao, Z. Shao, W. Shi, W. Li, Single-cell RNA sequencing reveals sexually dimorphic transcriptome and type 2 diabetes genes in mouse islet β cells. *Genom. Proteom. Bioinform.* **19**, 408–422 (2021).
40. A. T. Lun, K. Bach, J. C. Marioni, Pooling across cells to normalize single-cell RNA sequencing data with many zero counts. *Genome Biol.* **17**, 75 (2016).
41. A. T. Lun, D. J. McCarthy, J. C. Marioni, A step-by-step workflow for low-level analysis of single-cell RNA-seq data with Bioconductor. *F1000Res* **5**, 2122 (2016).
42. T. Stuart, A. Butler, P. Hoffman, C. Hafemeister, E. Papalexi, W. M. Mauck III, Y. Hao, M. Stoeckius, P. Smibert, R. Satija, Comprehensive integration of single-cell data. *Cell* **177**, 1888–1902.e21 (2019).
43. K. Van den Berge, H. R. de Bézieux, K. Street, W. Saelens, R. Cannoodt, Y. Saeys, S. Dudoit, L. Clement, Trajectory-based differential expression analysis for single-cell sequencing data. *Nat. Commun.* **11**, 1201 (2020).
44. H. Han, J. W. Cho, S. Lee, A. Yun, H. Kim, D. Bae, S. Yang, C. Y. Kim, M. Lee, E. Kim, S. Lee, B. Kang, D. Jeong, Y. Kim, H. N. Jeon, H. Jung, S. Nam, M. Chung, J. H. Kim, I. Lee, TRRUST v2: An expanded reference database of human and mouse transcriptional regulatory interactions. *Nucleic Acids Res.* **46**, D380–D386 (2018).

Acknowledgments: We thank W. Shi and T. Zhang for their technical support. **Funding:** This work was supported by funding sources as follows: National Key R&D Programmes of China 2020YFA0112500 (awarded to W.L.), 2016YFA0102200 (awarded to W.L.), 2018YFA0107102 (awarded to W.L.), and 2018YFA0107602 (awarded to Z.S.) as well as Key Project of the Science and Technology Commission of Shanghai Municipality, China grant no. 19JC1415300 (awarded to W.L.) **Author contributions:** Conceptualization: G.L., Y.L., Z.S., and W.L. Methodology: G.L., Y.L., and M.L. Resources: Q.H., S.-X.L., Q.S., X.C., and M.X. Investigation: G.L., Y.L., M.L., and S.L. Visualization: G.L., Y.L., and M.L. Supervision: Z.-N.Z., Z.S., and W.L. Writing (original draft): G.L. and Y.L. Writing (review and editing): Z.-N.Z., Z.S., and W.L. **Competing interests:** The authors declare that they have no competing interests. **Data and materials availability:** All data needed to evaluate the conclusions in the paper are present in the paper and/or the Supplementary Materials. Raw data (FASTQ files) for scRNA-seq are uploaded to GEO with accession number: GSE224572.

Submitted 9 December 2022

Accepted 18 April 2023

Published 24 May 2023

10.1126/sciadv.adg2183

Charting a high-resolution roadmap for regeneration of pancreatic β cells by in vivo transdifferentiation from adult acinar cells

Gang Liu, Yana Li, Mushan Li, Sheng Li, Qing He, Shuxin Liu, Qiang Su, Xiangyi Chen, Minglu Xu, Zhen-Ning Zhang, Zhen Shao, and Weida Li

Sci. Adv., **9** (21), eadg2183.
DOI: 10.1126/sciadv.adg2183

View the article online

<https://www.science.org/doi/10.1126/sciadv.adg2183>

Permissions

<https://www.science.org/help/reprints-and-permissions>

Use of this article is subject to the [Terms of service](#)

Science Advances (ISSN) is published by the American Association for the Advancement of Science. 1200 New York Avenue NW, Washington, DC 20005. The title *Science Advances* is a registered trademark of AAAS.
Copyright © 2023 The Authors, some rights reserved; exclusive licensee American Association for the Advancement of Science. No claim to original U.S. Government Works. Distributed under a Creative Commons Attribution NonCommercial License 4.0 (CC BY-NC).